Self-assembled $Co_3(BO_3)_2$/surfactant nanostructured multilayers

2001 J. Phys.: Condens. Matter 13 3913

(http://iopscience.iop.org/0953-8984/13/18/301)

INSTITUTE OF PHYSICS PUBLISHING JOURNAL OF PHYSICS: CONDENSED MATTER

J. Phys.: Condens. Matter **13** (2001) 3913–3921 www.iop.org/Journals/cm PII: S0953-8984(01)13829-4

Self-assembled $Co_3(BO_3)_2$/surfactant nanostructured multilayers

X X Zhang[1,4], Gang Gu[2], Houjin Huang[2], Shihe Yang[2] and Yuwei Du[3]

[1] Department of Physics and Institute of Nanoscience and Technology (INST), The Hong Kong University of Science and Technology, Clear Water Bay, Kowloon, Hong Kong
[2] Department of Chemistry, The Hong Kong University of Science and Technology, Clear Water Bay, Hong Kong
[3] National Laboratory of Solid State Microstructures and Dept of Physics, Nanjing University, Nanjing 210093, China

E-mail: phxxz@ust.hk

Received 9 May 2000, in final form 8 December 2000

Abstract

$Co_3(BO_3)_2$/surfactant composites have been prepared by the controlled precipitation of aqueous cobalt cations together with surfactant. The composite shows a layered structure as determined by x-ray diffraction, in which the $Co_3(BO_3)_2$ layers of about 6 Å in thickness are in alternation with surfactant bilayers. The temperature-dependent magnetization measured in the zero-field-cooled (ZFC) and field-cooled (FC) processes and the AC-magnetic susceptibility measured at different frequencies indicate that there is a freezing temperature at low temperature (<6 K) and the temperature is weakly frequency dependent. A clear difference between thermal remanent magnetization (TRM) and isothermal remanent magnetization (IRM) was observed at 2 K. All the experimental observations suggest that the multilayers are spinglass in nature.

Self-assembled (organized) materials may hold the key to developing new structures and devices in many advanced technology industries [1–3]. Structural order over many length scales can be created in self-organized materials by utilizing a host of molecular interactions including (i) hydrophobic and hydrophilic effects, (ii) hydrogen bonding, (iii) coulombic interactions and (iv) van der Waals forces [4]. Typical self-assembled materials tend to show structural periodicity on the nanometre scale (2–10 nm) [5]. This size regime gives materials many novel properties, which are intermediate between those observed in isolated atoms and those found in bulk solids. Nanostructured magnetic materials have been a very important field in the condensed materials physics, and have been fabricated through a diversity of ways. The synthesis of self-assembled inorganic/surfactant composites provides a versatile means to create nanostructured magnetic materials, which are of importance in both fundamental physics and applications [6]. Using this method, Tolbert *et al* synthesized ordered, lamellar

[4] Addressee for correspondence.

iron oxide/surfactant composites [6]. By varying the oxide layer thickness, very interesting magnetic behaviours have been observed. Other organic–inorganic transition metal layered magnetic materials studied quite intensively are the Mn(tetracyanoethylene)$_x$.y(CH_2Cl_2) [7] Fe(tetracyanoethylene)$_2$.y(CH_2Cl_2) [8] and $Cu_2(OH)_3(C_mH_{2m+1}COO)$, where $m = 7, 9$ and 11 [9]. Many interesting phenomena, such as ferromagnetic, antiferromagnetic, ferromagnetic and spin-glassy behaviours have been observed in these systems, and the physics behind the magnetic behaviours has been studied [7–9]. Two dimensional ferromagnetic materials of $MCu(opba)(DMSO)_3$, where M = Mn and Co have also been fabricated and studied [10, 11]. Thus the organic–inorganic transition metal layered magnetic nanocomposites provide us with a lot of new materials for both fundamental science and applications.

As well known, as the dimension(s) of a magnetic material decreases, the effects of the surface spins to its magnetic behaviour become more evident. A recent finding in this regard include fundamentally changed magnetic order in antiferromagnetic NiO nanoparticles due to the reduction in coordination of the surface spin [12], and the spin-glass-like surface in the γ-Fe_2O_3 ferrimagnetic nanoparticles [13]. The study of the self-assembled nanostructured magnetic materials is expected to shed light on the physics of the micro-magnetism [6, 14]. In this paper, we report the synthesis and magnetic properties of layered $Co_3(BO_3)_2$/surfactant composite. The material composed of $Co_3(BO_3)_2$ layers (∼6 Å) separated by non-magnetic surfactant layers (∼22 Å) shows a spin-glass-like behaviour which can be attributed to the spin disorder in the very thin $Co_3(BO_3)_2$ layers due to the reduction of the coordination of the surface spins [12] or the interactions among the $Co_3(BO_3)_2$ nanoclusters.

Self-assembled $Co_3(BO_3)_2$ multilayers were prepared by adding $CoCl_2.6H_2O$ to a diluted aqueous solution of sodium bis(2-ethylhexyl) sulphosuccinate ($C_{20}H_{37}O_7SNa$, in short, Na(AOT)), followed by mixing this solution with a $NaBH_4$ aqueous solution at room temperature in air. Briefly, 1.0 mmol Na(AOT) was first dissolved in 150 ml deionized water with a vigorous stir, and the solution was heated to 50 °C for 0.5 hour. After the solution was cooled to room temperature, 1.5 mmol $CoCl_{2.6}H_2O$ was added to it with a moderate stir. Then to this solution, 5 ml of a $NaBH_4$ solution (0.4 M) was added slowly with a slight stir. Concomitantly, a brown precipitate began to form. The precipitate (named as $Co_3(BO_3)_2$(AOT) hereafter) was filtered, washed with deionized water and dried in air at a temperature of 50 °C for 10 hours prior to measurements.

The powder XRD data of the samples prepared by the same procedure were collected from 2° to 80° (2θ) with Cu Kα for all our samples. The data are shown only in the range of 2° to 30° for the simplicity (figure 1). The XRD pattern (figure 1(a)) clearly demonstrates the layered structure of this inorganic/organic composite: a series of equally spaced peaks observed in the small angle range from 2° to 15°. The inset of figure 1(a) shows two broad diffraction peaks at larger angles (33.5° and 60.5°). These two peaks closely match the strongest (121) and moderately strong (330) diffraction peaks of orthorhombic $Co_3(BO_3)_2$. The broadness of the diffraction peaks signifies that the $Co_3(BO_3)_2$ size are in nm range. Elemental analysis gave B of 3.348% and Co of 22.8% in weight percentage, that is, the atomic ratio is B:Co∼1:1.3 consistent with that of $Co_3(BO_3)_2$. In order to gain further insight into the $Co_3(BO_3)_2$(AOT) structure, we also carried out XRD measurements on the sample before the reduction/oxidation treatment, i.e., Co(AOT). In figure 1(b), a much narrower peak compared to that in $Co_3(BO_3)_2$(AOT) is clearly observed. The narrowness of the single peak in Co(AOT) indicates that the layer spacing is quite precise, and the scattering factor modulation is nearly sinusoidal, which result in the appearance of only one narrow peak, whereas $Co_3(BO_3)_2$ (AOT) may possess sharper interfaces between the inorganic and organic layers, leading to appearance of the multiple broad peaks. The broadness of multiple peaks is likely to be caused by large variation in individual layer thickness. From the data, layer spacings of 2.78 nm and

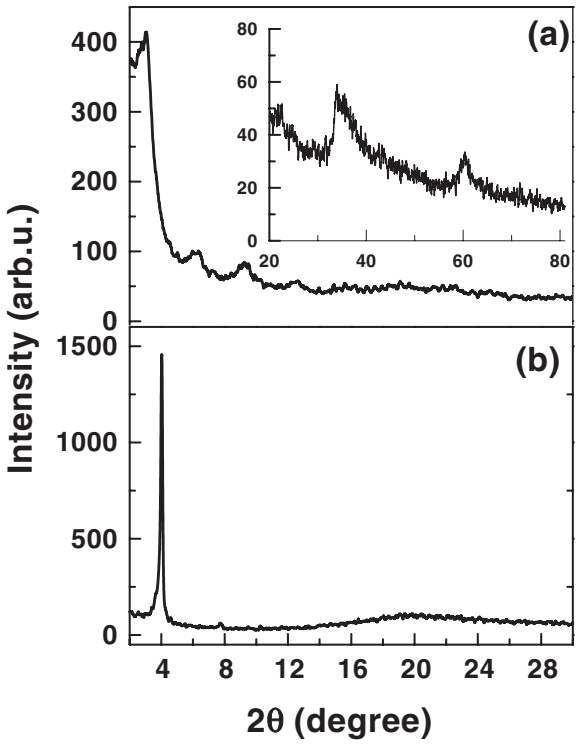

Figure 1. X-ray diffraction patterns obtained by Philips PW 1830 for: (a) $Co_3(BO_3)_2$(AOT); (b) Co(AOT).

2.18 nm are extracted for $Co_3(BO_3)_2$ (AOT) and Co(AOT) respectively. Considering that the layer spacing of $Co_3(BO_3)_2$(AOT) increases by about 6 Å compared to that of Co(AOT), we estimated that about two O–Co–O blocks are inserted in the surfactant layers [6]. A schematic representation of the $Co_3(BO_3)_2$ (AOT) structure is shown in figure 2, with each disordered cross linked $Co_3(BO_3)_2$ layer between two successive AOT layers.

Shown in figure 3 is the temperature-dependent magnetization in a small magnetic field of 100 Oe measured following the ZFC–FC procedure [15] using a SQUID magnetometer. It is obvious in figure 3 that the FC curve coincides with the ZFC curve only at high temperatures, and deviates from the ZFC curve at low temperatures, especially below the cusp of ZFC curve. This behaviour of the ZFC–FC curve is commonly observed in the spin-glass [16] and systems composed of interacting or non-interacting magnetic nanoclusters [15, 17]. By plotting $H/M(T)$ versus temperature in the high temperature range ($T > 15$ K), it is clear that the composite cannot be ascribed to the non-interacting superparamagnetic clusters. This is because $\chi(T)$ follows a Curie–Weiss law with $\theta = -95$ K, indicating an antiferromagnetic interaction or coupling between the magnetic ions or nanoclusters.

To clarify the physical origin of the peak in the ZFC curve and deviation between ZFC and FC curve at low temperature, the temperature dependence of AC-susceptibility was measured at different frequencies. Shown in figure 4 is the real part and imaginary part of AC-susceptibility χ' and χ'' versus temperature for different frequencies. It is obvious that the peaks in $\chi'(T)$ and $\chi''(T)$ shift to higher temperatures with increasing frequency of the AC-field, a characteristic behaviour of spin-glass and small magnetic particle systems [17–19]. For a system composed of

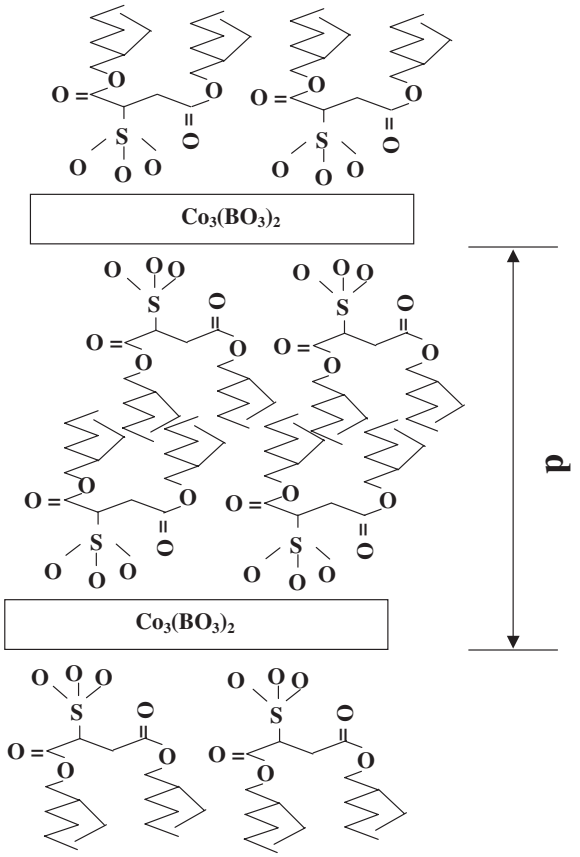

Figure 2. Schematic representation of the self-assembled $Co_3(BO_3)_2$ (AOT). The $Co_3(BO_3)_2$ layers ∼6 Å in thickness are separated by a 2.18 nm non-magnetic surfactant layer.

non-interacting, mono-dispersed, single domain magnetic particles, the two components of the susceptibility should be related by the Kramers–Kronig relation, and the relaxation time of the magnetic moment follows the Arrhenius law, $\tau = \tau_0 \exp(U/k_B T)$, where U is the anisotropy energy barrier for flipping the magnetic moment of the particle. τ_0 is the characteristic time of the system of the order 10^{-9} to 10^{-13} s [19]. It is known that when $\omega\tau = 1$, $\chi''(T)$ has a maximum (where $\omega = 2\pi f$, f is the frequency of AC-field), the temperature at which χ'' shows the maximum called the blocking temperature T_B. That is,

$$\ln 2\pi f = \ln\left(\frac{1}{\tau_0}\right) - \frac{U}{k_B T_B}. \tag{1}$$

Therefore, the values of T_B and the frequencies (f) used in the susceptibility measurement can be described by equation (1). Shown in the inset to figure 4(b) is the plot of $\ln(2\pi f)$ as a function of $1/T_P$, where the values of T_P were obtained from figure 4(b). It is clearly seen that these data has a perfect linear dependence, the dashed line is the least-square fitting data. The slope of the line is $U/k_B = 522$ K and the interception $\ln(1/\tau_0) = 80.6$ (s^{-1}), which leads to $\tau_0 = 10^{-35}$ s. It should be noticed that the extremely short characteristic time, $\tau_0 = 10^{-35}$ s, has never been observed in any magnetic systems. The shortest time scale in magnetism is the spin flip time of a single atom, $\tau_s = 10^{-13}$ s, no magnetic relaxation time scale should be

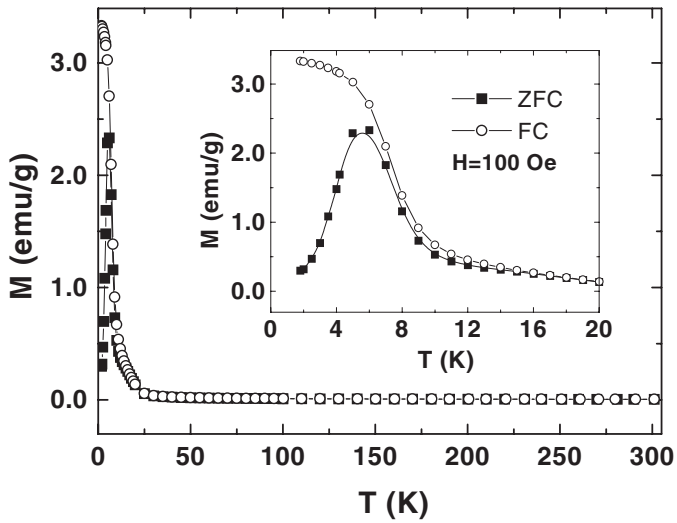

Figure 3. Temperature-dependent magnetization obtained in zero-field-cooled (ZFC) and field-cooled (FC) processes with an applied magnetic field of 100 Oe.

shorter than τ_s. Therefore the system could not be described by a system simply composed of non-interacting superparamagnetic clusters. There must be some strong interactions among the small clusters or spins which plays an important role in the freezing process of the magnetic moments at low temperatures.

On the other hand, this behaviour could be understood in the picture of the spin-glass [18] (the origin of the spin-glass in this system will be discussed later). Actually the superparamagnetic nanoparticles can also behave as a spin-glass when the interactions among the particles become strong enough, which was observed at low temperature in the frozen ferrofluid [17, 20]. One of the characteristics of the spin-glass is the difference between the thermal-remanent magnetization (TRM) and the isothermal-remanent magnetization (IRM) [18]. The values of TRM were obtained by field cooling the sample to a target temperature (2 K) from a temperature (50 K) much higher than the peak temperature in the ZFC curve, then the field was switched to zero and the remanent magnetization was measured. By repeating the above procedure using different applied magnetic fields, the field-dependent TRM was obtained. The field-dependent IRM was measured by cooling the sample from 50 K to 2 K in a zero field followed by cycling field $0 \rightarrow H \rightarrow 0$, and then measuring the magnetization. Figure 5 plots the field dependences of TRM and IRM. The difference between TRM and IRM is evident. Moreover, the behaviours of curves in figure 5 are in agreement with the fact that for a spin-glass, the saturation field for TRM is much smaller than that for IRM [18]. In addition to the spin-glassy characteristics revealed by the TRM and IRM, a logarithmic magnetic relaxation was found below 6 K. Shown in the inset to figure 5 is the magnetization as function of $\ln t$. The time-dependent magnetization data were obtained by cooling the sample in a 100 Oe field from 50 K to 2 K, then the field is switched off and the magnetization was measured in more 4000 s. It is obvious that the data can be described by $M(t) = M_0(1 - S \ln t)$, where S is the so-called magnetic viscosity [16]. The high temperature isothermal magnetization as function of H/T is shown in figure 6. It is evident that the curves do not collapse to a master curve, which indicates again that the system is not composed of non-interacting superparamagnetic clusters [21]. Figure 7 plots the coercive field as a function of the square

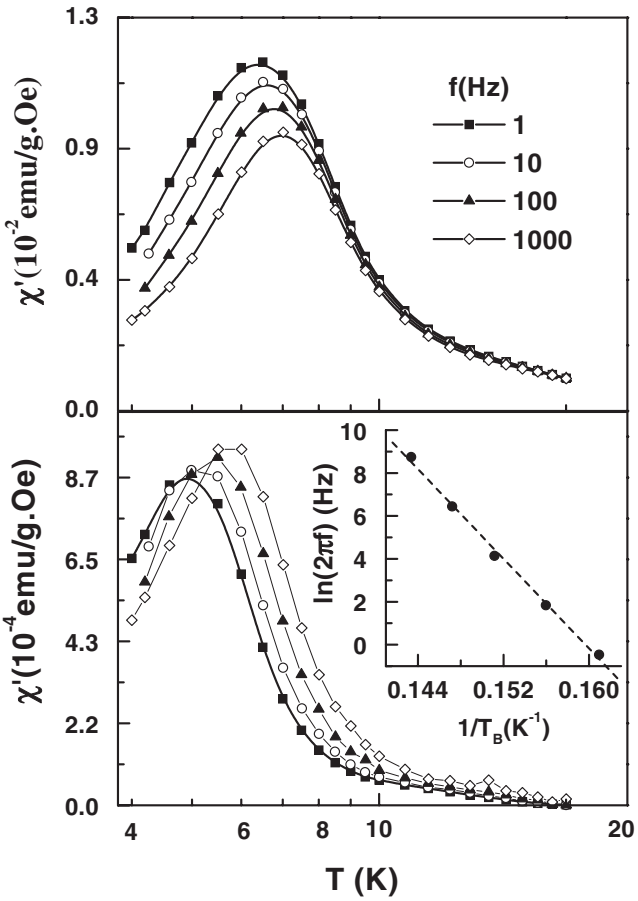

Figure 4. Temperature dependent magnetic AC-susceptibility, $\chi(T) = \chi'(T) + \mathrm{i}\chi''(T)$, obtained at different frequencies in a zero DC field: (a) real part $\chi'(T)$ and (b) imaginary part. Shown in the inset to (b) is the plot of $\ln(2\pi f)$ as a function of $1/T_p$. A perfect linear dependence is evident, the line is the fitting data.

root of temperature $T^{1/2}$, for $T < 6$ K. As it is well known that for the non-interacting (or weakly interacting) magnetic clusters (particles) the temperature dependence of coercive field $H_C(T)$, below the blocking temperature T_B, is dominated by superparamagnetic relaxation which leads to $H_C(T) = H_C(0)(1 - \sqrt{T/T_B})$ [22]. It is obvious that the data shown in figure 7 do not follow the $\sqrt{T}$ dependence.

Bulk $Co_3(BO_3)_2$ is an antiferromagnet with the Néel temperature $T_N = 30$ K [23], and it is of kotoites type crystalline structure with $a = 5.46(2)$, $b = 8.43(6)$ and $c = 4.64(8)$ Å [23]. The neutron-diffraction data indicate the magnetic unit cell can be indexed as $\boldsymbol{a}$, $2\boldsymbol{b}$, $2\boldsymbol{c}$, therefore it is four times the size of the chemical cell [23, 24].

Since the layer thickness of $Co_3(BO_3)_2$ in our materials is ~6 Å, which is less than the edge length of its magnetic unit cell, the finite size effect may lead to the formation of a magnetic spin-glass very easily [25], as observed in the ferrimagnetic γ-Fe_2O_3 [13] nanoparticles. Our sample may have a similar situation as in the antiferromagnetic NiO nanoparticles, where the magnetic order is changed fundamentally by reduced coordination of surface spins [12]. Therefore, the frustration of the spin couplings in the $Co_3(BO_3)_2$ layers (less than 1 nm) should

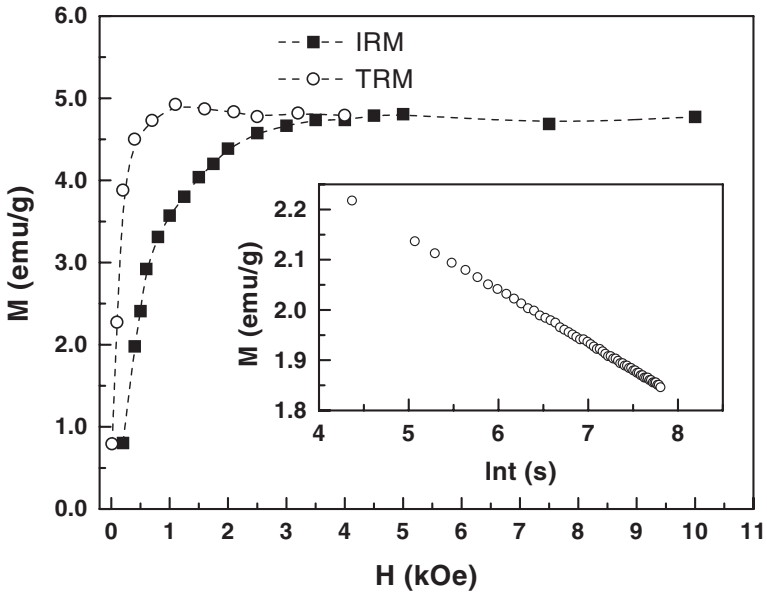

Figure 5. Values of thermal remanent magnetization (TRM) and isothermal remanent magnetization (IRM) as a function of applied magnetic fields obtained at 2 K. The inset plots the time-dependent magnetization as a function of $\ln t$ obtained at 2 K.

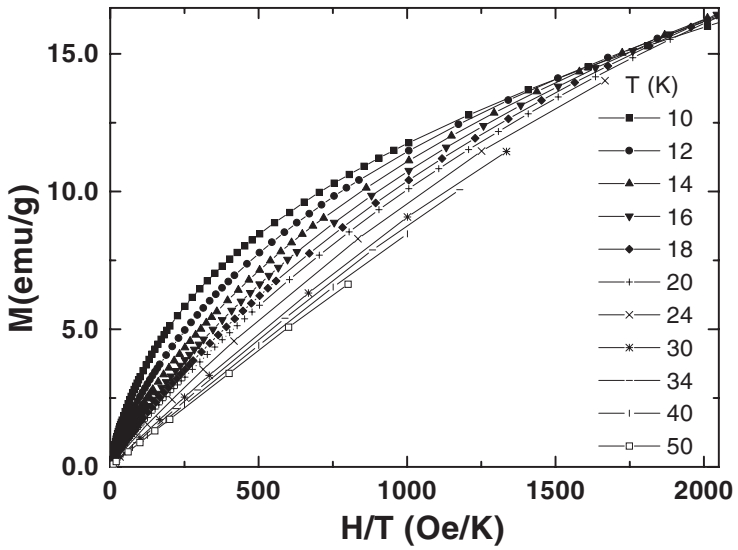

Figure 6. Isothermal magnetization M against H/T for different temperatures ($T > 8$ K). The curves do not collapse to a master curve, an indication that the system is not composed of superparamagnetic particles.

be expected, which may lead to a transformation from antiferromagnetism to a spin-glass behaviour [12, 13].

In summary, self-assembled $Co_3(BO_3)_2$/surfactant nanostructured multilayers were studied using AC-susceptibility measurement, temperature dependence of magnetization

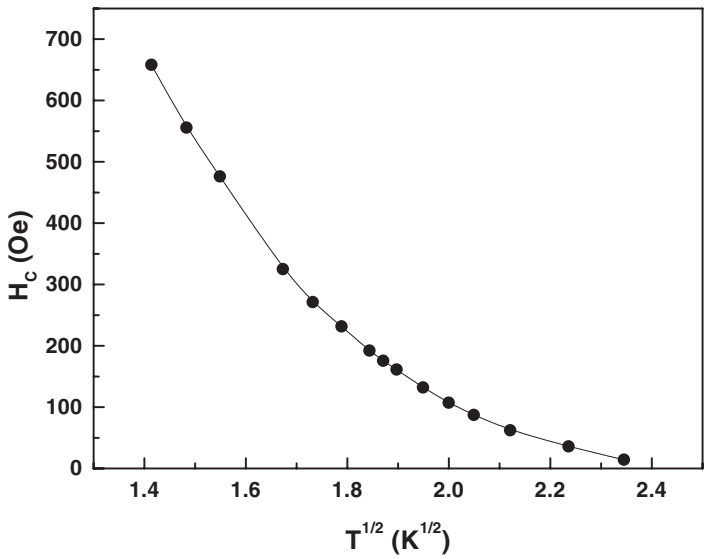

Figure 7. Coercive fields H_C, measured at $T < 6$ K, plotted as a function of $\sqrt{T}$.

(ZFC–FC) and field dependence of magnetization ($M(H)$, coercive field, TRM and IRM)). All these observations clearly suggest that the materials can be described in the term of spin-glass rather than a system composed of non-interacting (superparamagnetic) magnetic particles.

Acknowledgments

Support from RGC of Hong Kong (HKUST6190/99P and HKUST6111/98P) and HKUST (HIA programme) is gratefully acknowledged.

References

[1] Muthukumar M, Ober C K and Thomas E L 1997 *Science* **277** 1225 and references therein
[2] Zhong-Renchen *et al* 1997 *Science* **277** 1248 and references therein
[3] Decher G 1997 *Science* **277** 1232
[4] Whitesides G M, Mathias J P and Seto C T 1991 *Science* **254** 1312
[5] Kresge C T *et al* 1992 *Nature* **359** 710
[6] Tolbert S H *et al* 1997 *J. Am. Chem. Soc.* **119** 8652
[7] Wynn C M, Girtu M A, Zhang J, Miller J S and Epstein A J 1998 *Phys. Rev.* B **58** 8508
[8] Girtu M A, Wynn C M, Zhang J, Miller J S and Epstein A J 2000 *Phys. Rev.* B **61** 492
[9] Girtu M A, Wynn C M, Fujita W, Awaga K and Epstein A J 2000 *Phys. Rev.* B **61** 4117
[10] Cador O *et al* 1997 *J. Mater. Chem.* **7** 1263
[11] Kahn O 2000 *Acc. Chem. Res.* **33** 647
[12] Kodama R H, Markhlouf S A and Berkowitz A E 1998 *Phys. Rev. Lett.* **79** 1393
[13] Martinez B *et al* 1998 *Phys. Rev. Lett.* **80** 181
[14] Yin J S and Wang Z L 1997 *Phys. Rev. Lett.* **79** 2570
[15] Zhang X X, Hernandez J M, Tejada and Ziolo R F 1996 *Phys. Rev.* B **54** 4101
[16] Tejada J, Zhang X X and Chudnovsky E M 1993 *Phys. Rev.* B **47** 14 977
[17] Jonsson T *et al* 1995 *Phys. Rev. Lett.* **75** 4138
[18] Mydosh J A 1993 *Spin Glass: an Experimental Introduction* (London: Taylor and Francis)
[19] Dormann J L, Fiorani D and Tronc E 1998 *Adv. Chem. Phys.* **98** 283
[20] Luo Weili 1991 *Phys. Rev. Lett.* **67** 2721

[21] Majetich S A *et al* 1993 *Phys. Rev.* B **48** 16 845
[22] Kneller E F and Luborsky F E 1963 *J. Appl. Phys.* **34** 656
Xiao G and Chien C L 1987 *Appl. Phys. Lett.* **51** 1280
Chien C L 1991 *J. Appl. Phys.* **69** 5267
[23] Newnham R E, Santoro R P, Seal R F and Stallings G N 1966 *Phys. Status Solidi* **16** K17
[24] Newnham R E, Redman M J and Santoro R P 1965 *Z. Kristallogr.* **121** 418
[25] Fischer K H and Hertz J A 1991 *Spin Glasses* (Cambridge: Cambridge University Press) p 2